A&A 487, 697–707 (2008)
DOI: 10.1051/0004-6361:200809779

Astronomy & Astrophysics

From B[e] to A[e]

On the peculiar variations of the SMC supergiant LHA 115-S 23 (AzV 172)

M. Kraus[1], M. Borges Fernandes[2,3], J. Kubát[1], and F. X. de Araújo[4]

[1] Astronomický ústav, Akademie věd České republiky, Fričova 298, 251 65 Ondřejov, Czech Republic
e-mail: [kraus;kubat]@sunstel.asu.cas.cz
[2] Royal Observatory of Belgium, Ringlaan 3, 1180 Brussels, Belgium
[3] UMR 6525 H. Fizeau, Univ. Nice Sophia Antipolis, CNRS, Observatoire de la Côte d'Azur, Av. Copernic, 06130 Grasse, France
e-mail: Marcelo.Borges@obs-azur.fr
[4] Observatório Nacional, Rua General José Cristino 77, 20921-400 São Cristovão, Rio de Janeiro, Brazil
e-mail: araujo@on.br

Received 14 March 2008 / Accepted 1 June 2008

ABSTRACT

Context. Optical observations from 1989 of the Small Magellanic Cloud (SMC) B[e] supergiant star LHA 115–S 23 (in short: S 23) revealed the presence of photospheric HeI absorption lines, classifying S 23 as a B8 supergiant. In our high-resolution optical spectra from 2000, however, we could not identify any HeI line. Instead, the spectral appearance of S 23 is more consistent with the classification as an A1 supergiant, maintaining the so-called B[e] phenomenon.
Aims. The observed changes in spectral behaviour of S 23 lead to different spectral classifications at different observing epochs. The aim of this research is, therefore, to find and discuss possible scenarios that might cause a disappearance of the photospheric HeI absorption lines within a period of only 11 years.
Methods. From our high-resolution optical spectra, we perform a detailed investigation of the different spectral appearances of S 23 based on modern and revised classification schemes. In particular, we derive the contributions caused by the interstellar as well as the circumstellar extinction self-consistently. The latter is due to a partly optically thick wind. We further determine the projected rotational velocities of S 23 in the two epochs of spectroscopic observations.
Results. Based on its spectral appearance in 2000, we classify S 23 as A1 Ib star with an effective temperature of about 9000 K. This classification is supported by the additional analysis of the photometric UBV data. An interstellar extinction value of $E(B-V) \simeq 0.03$ is derived. This is considerably lower than the previously published value, which means that, if the circumstellar extinction due to the stellar wind is neglected, the interstellar extinction, and hence the luminosity of the star, are overestimated. We further derive a rotation velocity of $v \sin i \simeq 150$ km s^{-1}, which means that S 23 is rotating with about 75% of its critical speed. The object S 23 is thus the fourth B[e] supergiant with confirmed high projected rotational velocity. The most striking result is the apparent cooling of S 23 by more than 1500 K with a simultaneous increase of its rotation speed by about 35% within only 11 years. Since such a behaviour is excluded by stellar evolution theories, we discuss possible scenarios for the observed peculiar variations in S 23.

Key words. stars: fundamental parameters – stars: winds, outflows – supergiants – stars: individual: LHA 115-S 23 (AzV 172)

1. Introduction

B[e] stars belong to one of the puzzling phenomena in modern astrophysics. While many of their members have been known for decades, the number of new detections of B[e] stars is growing tremendously (see, e.g., Kraus & Miroshnichenko 2006). The classification by Lamers et al. (1998) of B[e] stars according to their evolutionary phase made clear that B[e] stars occur in the pre- as well as in the post-main sequence phase, and the most popular class is formed by the B[e] supergiants with confirmed members predominantly in the Magellanic Clouds (see the recent review by Zickgraf 2006).

The derivation of stellar parameters of B[e] stars is complicated because in most cases the stellar photospheres are hidden inside the dense and optically-thick winds. Thus, the spectra are contaminated with wind continuum emission in the form of free-free and free-bound emission as well as with an enormous amount of emission lines that are generated in the circumstellar wind material, which is usually non-spherically symmetric. Evidence for non-sphericity thereby comes from polarimetric observations, e.g., by Magalhães (1992), Magalhães et al. (2006), and Melgarejo et al. (2001), in rare cases even from optical imaging with the Hubble Space Telescope, as was the case for the galactic B[e] star Hen 2–90 (Sahai et al. 2002; Kraus et al. 2005), and from interferometric observations with, e.g., the VLTI/AMBER and VLTI/MIDI instruments (e.g., Domiciano de Souza et al. 2007). An observed strong infrared (IR) excess emission due to warm and hot circumstellar dust (e.g., Zickgraf et al. 1985, 1986, 1989, 1992; Gummersbach et al. 1995, Borges Fernandes et al. 2007) indicates the presence of a high-density disk. This disk must further be the location of the neutral material like OI (Kraus et al. 2007) and the molecular gas, expressed by CO first-overtone bands (McGregor et al. 1988a, 1988b, 1989; Morris et al. 1996; Kraus et al. 2000) and TiO band emission (Zickgraf et al. 1989). The proposed scenario for B[e] supergiants thus suggests that their circumstellar material consists of a disk-like structure formed by a high density equatorial wind with low outflow velocity, and a normal B-type line-driven wind of high velocity and much lower density in polar directions (Zickgraf et al. 1985; Zickgraf 2006). A possible mechanism for

the formation of outflowing high density disks might be rapid rotation of the central star (see, e.g., Bjorkman & Cassinelli 1993; Curé 2004; Curé et al. 2005). In addition, if the star is rotating rapidly, the wind material in the equatorial plane recombines in hydrogen in the vicinity of the stellar surface, as has recently been shown by Kraus (2006). And for at least three B[e] supergiants projected rotational velocities at a significant fraction of their critical speed have indeed been found (Gummersbach et al. 1995; Zickgraf 2000, 2006), hinting to the possible connection between the presence of a circumstellar disk and stellar rotation.

For the Small Magellanic Cloud (SMC) star LHA 115-S 23 (AzV 172, 2MASS J00555380–7208596, in the following refered to as S 23) that is investigated in this paper, no rotational velocity has been derived yet. In addition, not much is known about the orientation of the system, although it has been suggested to be seen more or less edge-on, based on the low expansion velocity derived from the Balmer lines (Zickgraf et al. 1992, referred to as ZSW in the following). This object was first classified by Azzopardi & Vigneau (1982) as a B8 supergiant, and the detection of several photospheric HeI absorption lines in the optical mid-resolution spectrograms of ZSW is in agreement with the classification of S 23 as a late B-type supergiant. These authors further fixed the interstellar extinction at $E(B-V) = 0.10$, derived an effective temperature of $T_{\rm eff} = 11\,000$ K, and a surface gravity of $\log g = 2.0$. This led to $M_{\rm bol} = -6.4$, $\log L_*/L_\odot = 4.46$, $R_* = 45\,R_\odot$, and the assignment of the luminosity class Ib. The spectra of ZSW showed further strong Balmer line emission, [OI] emission, as well as many FeII and [FeII] emission lines. In combination with the pronounced infrared excess in the photometric data, which can be ascribed to warm or hot circumstellar dust, ZSW assigned S 23 to the group of B[e] supergiants.

About eleven years later, during our observing mission of Magellanic Cloud B[e] supergiants, we observed S 23 using a high-resolution optical spectrograph. Our spectra confirm the presence of the strong Balmer emission lines as well as of the [OI], [FeII], and FeII emission lines. But interestingly, even with a more than 10 times higher resolution, our spectra do not display any HeI line either in absorption nor in emission. The absence of the HeI lines speaks more in favour of a cooler central object than a late B supergiant. This paper is therefore aimed to investigate in detail the spectral appearances of S 23 at the two epochs of observations and to discuss possible scenarios that might cause the observed peculiar variations of S 23.

The paper is structured as follows: our observations are described in Sect. 2. Then, we perform the spectral classification of S 23 for the two different observing epochs, using modern, improved classification schemes (Sect. 3) and determine the contributions of both, interstellar and circumstellar extinctions (Sect. 4). From the detected photospheric MgII absorption lines, we next derive the projected rotation velocity of S 23 at the two epochs of observations (Sect. 5). In Sect. 6, we discuss possible scenarios that might explain the observed peculiarities, before we summarise our major results in Sect. 7.

2. Observations

We obtained the optical spectra with the 1.52-m telescope at the European Southern Observatory in La Silla (Chile) using the high resolution Fiber-fed Extended Range Optical Spectrograph (FEROS). FEROS is a bench-mounted Echelle spectrograph with fibers, which covers a sky area of 2″ of diameter, with a wavelength coverage from 3600 Å to 9200 Å and a spectral resolution of $R = 55\,000$ (in the region around 6000 Å). We adopted its complete automatic on-line reduction. The high-resolution spectrum of S 23 was taken on October 14, 2000, with an exposure time of 3600 s. The S/N ratio in the 5500 Å region is approximately 40. Since within the same night we were able to take two consecutive spectra of the star, which do not show significant differences, we added them up for a better S/N ratio achievment.

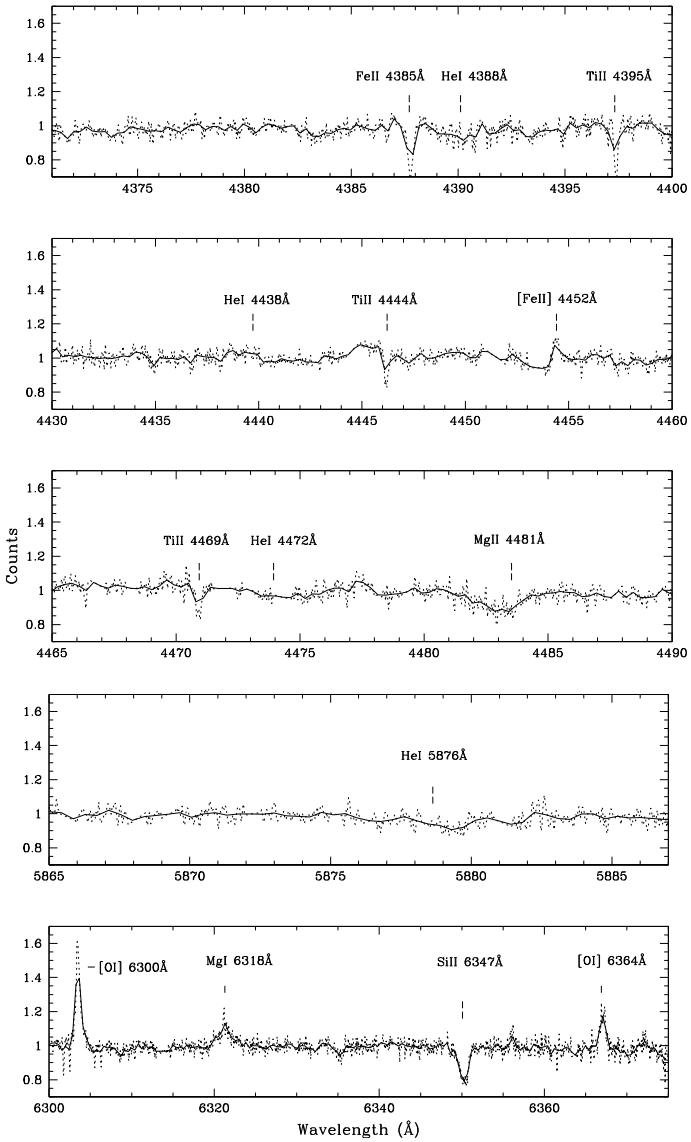

Fig. 1. Parts of the rectified FEROS spectrum (dashed lines) showing the regions around several expected HeI lines. For better visualization, we convolved the FEROS data to a resolution of $R = 4900$ as was used by ZSW (solid lines).

In Fig. 1, we display parts of the rectified high-resolution FEROS spectra. The first three panels show the regions around the positions of several HeI lines, which were identified by ZSW in their 1989 low-resolution (i.e. $R = 4900$) observations (see Fig. 4 of ZSW), with the HeI λ4472 line being the strongest one with almost equal equivalent width to the adjacent MgII λ4481 line. This HeI line is clearly absent in our FEROS spectrum (or at least below the detection limit) as well as the other two HeI lines at $\lambda\lambda$4388, 4438, whose detection was previously reported. The fourth panel of Fig. 1 displays the region around the HeI λ5876 line. If HeI is present in a stellar spectrum, then this line is usually quite strong. But obviously, it is also absent from our

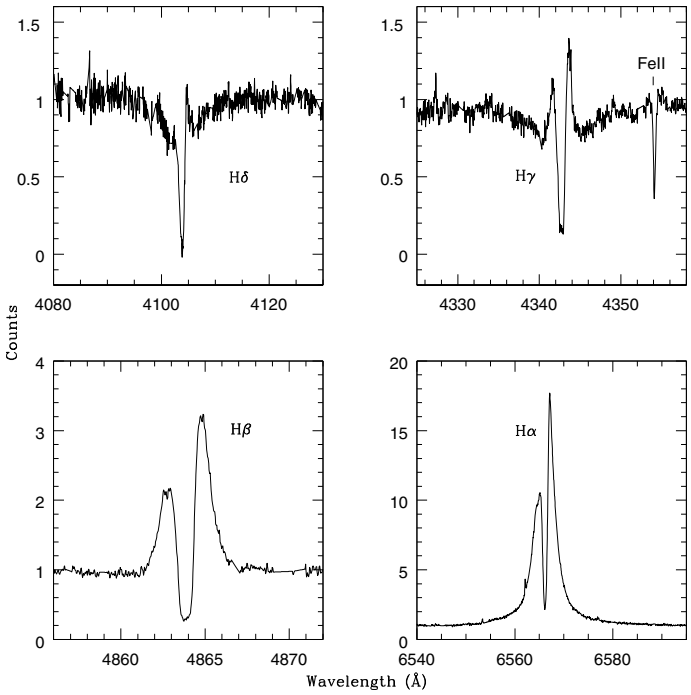

Fig. 2. Balmer lines in the spectrum of S 23.

FEROS spectrum. We checked the complete FEROS spectrum, but we could not identify a single HeI line.

Due to our rather low S/N ratio and the fact that the photospheric HeI absorption lines are expected to be broad and shallow, the high-resolution spectrum might not be able to display these lines properly. Instead, for these lines a (much) lower spectral resolution might be advantageous as has been shown by Verschueren (1991). We therefore convolved our data to the same resolution as the ZSW spectrum and overplotted the low-resolution spectrum in Fig. 1. However, even with the low-resolution data, the HeI lines do not show up.

While other known B[e] supergiants do not display even a single photospheric absorption line in their optical spectra due to their high density and therefore optically thick winds, S 23 displays at least one clearly detectable line, namely the MgII doublet at λ4481. And also the higher Balmer lines (Hδ, Hγ, see Fig. 2), as already mentioned by ZSW, show indications for a photospheric absorption component on which P Cygni profiles seem to be superimposed. Some other lines in our spectra also display absorption components, like FeII, TiII, and SiII (see Fig. 1). These absorption components are, however, much narrower than the MgII line, indicating that they are circumstellar in origin.

We measure the heliocentric radial velocity for several lines in our spectra: from the narrow pure emission lines of the forbidden transitions (like [OI], [FeII], see Fig. 1), from the narrow absorption components observed for most of the permitted transitions (like FeII, and two lines of SiII and CrII), and from the narrow absorption components of the Balmer lines[1]. For each element we derive mean values, which are listed in Table 1. For comparison, we also included in this table the values obtained by ZSW. While our metal lines all deliver values in the range

[1] For the Balmer lines, we list the mean radial velocity derived from the central absorption component for 4 lines (Hβ, Hγ, Hδ and Hϵ–Hβ and Hϵ were not observed by ZSW), while for Hα the radial velocity derived for the central absorption (^{ca}), the red peak (^{rp}), and the blue peak (^{bp}) are given.

Table 1. Mean heliocentric radial velocities derived from different ions compared to those derived by ZSW.

Ion	v_{rad} (km s^{-1})	v_{rad}^{ZSW} (km s^{-1})
[Fe II]	156.9	141.0
[O I]	156.1	164.0
Si II	155.7	150.0
Fe II	159.9	144.0
Cr II	161.1	–
Balmer lines	152.8	143.0
Hα^{ca}	150.9	126.0
Hα^{bp}	110.0	70.0
Hα^{rp}	197.0	210.0

155 . . . 160 km s^{-1}, the values of ZSW indicate a much larger scatter between the radial velocities of the forbidden and the pemitted lines, which had been interpreted by these authors as a slow outflow component. In fact, the narrow absorption components of the permitted lines, often overlaid on broader emission components, are not of pure atmospheric origin. Instead, they are generated due to absorption by the circumstellar material. The same holds also for the narrow absorption components seen in the Balmer lines. For a proper radial velocity determination we therefore rely on forbidden lines, which display narrow but symmetrical line profiles. From these lines, we thus obtain a mean radial velocity of $v_{rad} = 156.5 \pm 1.0$ km s^{-1}, which we will use here. It is slightly lower than the value found by ZSW from their [OI] lines, but this might be a spectral resolution effect rather than a stellar effect.

The largest difference between the ZSW and our data is reached by the two emission peaks of the Hα line. Here, a clear shift in velocities is present. This shift is about 40 km s^{-1} for the blue peak, while it is only 10–15 km s^{-1} for the red peak. We tested the influence of the different resolutions by smearing our Hα line to the same resolution as ZSW. The measured radial velocities are in much better agreement with the ZSW values, so that we can conclude that the differences in the appearance of the Hα line in ZSW and in our spectrum are most probably caused by the different spectral resolutions.

3. Spectral classification of S 23

3.1. Temperature classification

The determination of the spectral type and luminosity class of stars with metallicities different from the galactic one has been found to be a difficult task in the past. The reason for this is the fact that with decreasing metallicity the metal lines in the spectra become very weak and hard to detect. The proper determination of the spectral type is rather complicated, especially for B-type stars which do not or only very weakly show HeII lines in their spectra. For these objects, the classification has to be performed with the help of the metal lines and is, for galactic objects, normally based on the line strengths of silicon and magnesium, usually in comparison to helium. As shown, e.g., by Lennon et al. (1993) for galactic B supergiants, the equivalent widths of many spectral lines show a typical behaviour with spectral type, i.e. effective temperature. And later on, Lennon (1997) suggested determining the spectral classes of B-type supergiants in the SMC according to line ratios in such a way that the same trend in line ratios with spectral type is achieved as for solar metallicity (Lennon et al. 1992). His classification scheme (see Table 1 of Lennon 1997), which has been extended

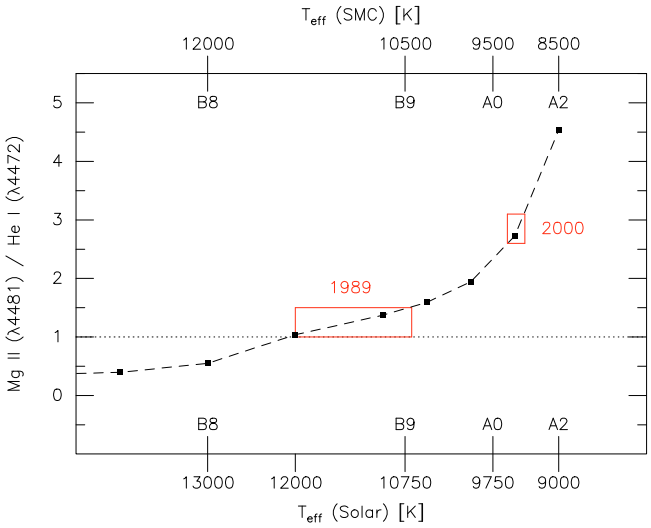

Fig. 3. Effective temperature dependence of the line ratio MgII λ4481 over HeI λ4472 calculated from model stellar atmospheres with $\log g = 2.5$ at solar abundances. The behaviour between spectral type and effective temperature taken from Evans & Howarth (2003) is indicated in the bottom label for solar abundance, and in the top label for SMC abundance. The two boxes indicate the observed ratios with their errors for the ZSW spectrum taken in 1989 and our spectrum taken in 2000, respectively.

to G-type stars by Evans et al. (2004), is used by many authors to classify B-type supergiants in many galaxies with abundances similar to the SMC value (e.g., Evans & Howarth 2003; Bresolin et al. 2006; Bresolin et al. 2007).

The spectral type of S 23 has been determined by Azzopardi & Vigneau (1987) as B8, and later on, ZSW, derived an effective temperature of about 11 000 K based on comparison of the observed spectral energy distribution to Kurucz (1979) model atmospheres. Inspection of their mid-resolution spectrum indicates the presence of the HeI λ4472 and MgII λ4481 lines, with the MgII line being slightly stronger than the HeI line. Lennon et al. (1993) already mentioned the sharp decrease in HeI equivalent width from early to late B-type supergiants, and the simultaneous strong increase in MgII λ4481 equivalent width. The relative strength of these two lines is therefore one of the main classification characteristics of especially late B-type supergiants (e.g., Bresolin et al. 2006; Lennon 1997). According to the classification scheme of Lennon (1997), the line ratio as inferred from the ZSW spectrum would thus suggest a spectral type between B8 and B9 of S 23 in the year 1989.

Our own high-resolution spectra display only the MgII λ4481 line while the adjacent HeI λ4472 line is definitely below the detection limit. This would speak more in favour of a star with spectral type A0 or later. To quantify these classifications and to constrain the possible range in effective temperature at the two observing epochs, it is necessary to calculate theoretical line ratios of MgII λ4481 over HeI λ4472. This is done by using the code SYNSPEC (see Hubeny & Lanz 2000) to compute line identification tables based on Kurucz (1979) model atmospheres in local thermodynamical equilibrium (LTE) and Kurucz (1993) line lists. These calculations have been performed for effective temperatures ranging from 8000 K up to 15 000 K and solar abundances. With these line identification tables that contain information about the expected line equivalent widths, we then calculated the MgII λ4481 over HeI λ4472 line ratios. The results are shown as the dashed line in Fig. 3. To convert the effective temperature scale into a spectral type, we made use of the recent classification of Evans & Howarth (2003), who redefined effective temperatures for galactic (indicated along the bottom axis of Fig. 3) and SMC supergiants (indicated along the top axis). In addition, we follow the approach of Lennon (1997), who suggested that the same line ratio mirrors the same spectral type. We find that the transition from a line ratio smaller than one to a ratio larger than one happens at an effective temperature of about 12 000 K for solar abundances, which corresponds to a spectral type between B8 and B9, in agreement with what has been claimed by Lennon (1997).

Concerning the measured line ratios of S 23 we could derive a value of 1.25 ± 0.25 from the low-resolution spectrum of ZSW[2]. This value, with its error, is included in Fig. 3. Its location in the diagram indicates that in 1989 the spectrum of S 23 was that of a B8.5–B9 star with effective temperature $T_{\rm eff} \simeq (11\,000 \pm 500)$ K. This classification is in fair agreement with the one derived by ZSW.

From our own spectrum taken in 2000, we derive a line ratio of 2.85 ± 0.25. This ratio has to be considered as a lower limit since we used, for the equivalent width of the HeI λ4472 line, the value we consider the detection limit. With this line ratio, we therefore determine an upper limit to the effective temperature that is mirrored by this line ratio. We find, for S 23, a spectral type later than A0 and an effective temperature $T_{\rm eff} \lesssim 9500$ K. If the spectral appearance of S 23 at the two observing epochs is indeed determined by the temperature of the central star, then the change in line ratio suggests that the star must have cooled by at least 1500 K within a period of 11 years only, a scenario that is definitely excluded by stellar evolution theory (see Sect. 6.1). In the following, we will therefore refer to this behaviour as an *apparent* cooling of the star.

3.2. Luminosity class

For the SMC, great effort has been undertaken for a proper luminosity classification of the supergiant population. In principle, several methods for the determination of the stellar luminosity exist and have been successfully applied in the literature. For O-type to early B-type supergiants, the HeI/HeII line ratios are good and, especially, metallicity-independent luminosity indicators (e.g., Walborn 1983). For B and later type supergiants, the Hγ equivalent width is an ideal and metallicity-independent tool for the luminosity class determination, as shown by Azzopardi (1987), while the use of metal lines as suggested by Massey et al. (1995) delivers unreliable results when applied to stars in low-metal content galaxies like the SMC (see the discussion in Lennon 1997).

For S 23, the luminosity class determination is complicated due to fact that its Hγ line shows an additional emission component (see Fig. 2). In this case, the equivalent width method of Azzopardi (1987) is not applicable.

ZSW had derived the luminosity class Ib from determining $E(B-V)$ based on the photometric B and V data of S 23 from Azzopardi & Vigneau (1982). Using the intrinsic colors for a B8 supergiant from Schmidt-Kaler (1982), they found a value of $E(B-V) = 0.10$. However, as we will show in Sect. 4, this extinction determination is based on assumptions that are not reliable for typical B[e] stars, and consequently, the $E(B-V)$ value

[2] This value has been derived by hand from the published spectrum because the digital spectra are not available anymore (Zickgraf, private communication).

Table 2. Photometric data of S 23 (in mag) collected from the literature and sorted by their year(s) of observation.

Year	U	B	V	R	J	H	K/K_s	References
1972–74	13.27	13.43	13.37	–	–	–	–	Azzopardi & Vigneau (1982)
1988	–	–	–	–	13.04	12.79	12.16	Zickgraf et al. (1992)
1998	–	–	–	–	13.02	12.76	12.15	Skrutskie et al. (2006, 2MASS)
1999	13.11	13.38	13.31	13.19	–	–	–	Massey (2002)

derived by ZSW *overestimates* the real amount of interstellar extinction and, therefore, the luminosity of S 23.

From our FEROS spectrum alone, we are not able to make any estimates about the stellar luminosity. We therefore searched the literature for complementary photometric data. These data, which have usually errors on the order of 0.01 mag, are summarised in Table 2, and the K_s band belongs to the 2MASS observations. Inspection of this table delivers the following important information:

- the UBV data of S 23 have changed substantially between the observations taken in 1972–74 and those taken in 1999, while the near-IR photometry appears constant in the measurements taken in 1988 and in 1998;
- the UBV data of Azzopardi & Vigneau (1982) were taken 14–16 years *before* ZSW took their near-IR data. With the knowledge of a possible variation/cooling of the central star as discussed above, the combination of these two datasets for the construction of the spectral energy distribution is therefore most certainly unreliable;
- in 1999, the star appears to be more luminous in the UBV bands than it was during the 1972–74 observing period;
- the UBV data of Massey (2002) were taken only one year earlier than our FEROS spectra, and we use them as complementary data to our optical spectra for a tentative luminosity determination.

From the photometry of Massey (2002) we can estimate the luminosity class of S 23 in the year 1999, if we completely neglect the interstellar extinction towards S 23 for the moment. From the distance modulus of $\mu = 18.93$ (Keller & Wood 2006), we thus find a first-guess absolute visual magnitude of $M_V = -5.62$, assigning to S 23 the luminosity class Ib.

4. Interstellar and circumstellar extinction

In the previous section, we determined the luminosity class of S 23 as Ib. For this, we ignored the presence of any interstellar extinction value, knowing that this delivers only a lower limit to the real stellar luminosity. In this section, we therefore intend to derive the values of the interstellar and possible circumstellar extinction. This is necessary for a proper dereddening of the photometric data and a reliable stellar luminosity determination.

To derive $E(B-V)$ from the color index of a star, one should not only rely on the $B-V$ color index, but also check, if possible, the result by using a different color index, e.g. $U-B$. The observed colors from Azzopardi & Vigneau (1982) given in Table 2 serve as an example. According to the classification of S 23 as B8 Ib, ZSW derived a value of $E(B-V) = 0.10$ from $(B-V)$. Using as well the color index $(U-B)$, and the intrinsic color of Johnson (1966), we find an extinction of $E(B-V) = 0.49$. For the calculation of this value, we used the relation $E(B-V) = E(U-B)/0.77$, which has been found from observations by Leitherer & Wolf (1984). The value found from the $U-B$ color index thus seems to indicate an extinction five times higher.

One might argue that, since the star seems to be somehow variable, the spectral type derived from the optical data of ZSW cannot be applied to the UBV data taken about 14 years earlier. Therefore, we checked the possible interstellar extinction values derived from the more recent set of UBV data from Massey (2002), using the spectral classification derived from our optical spectra that have a time offset of about one year, only.

From Fig. 3, we found the spectral type of S 23 as A0 or later, and in the following we will deal with two stellar scenarios, namely an A0 Ib star with $T_{\rm eff} = 9500$ K, and an A1 Ib star with $T_{\rm eff} = 9000$ K. Using the tables with intrinsic colors from Johnson (1966), we find the following extinction values:

$$E(B-V) = \left\{ \begin{matrix} 0.06 \\ 0.18 \end{matrix} \right\} \quad \text{from} \quad \left\{ \begin{matrix} (B-V) \\ (U-B) \end{matrix} \right\} \quad \text{for} \quad \text{A0 Ib}\,,$$

and

$$E(B-V) = \left\{ \begin{matrix} 0.04 \\ 0.07 \end{matrix} \right\} \quad \text{from} \quad \left\{ \begin{matrix} (B-V) \\ (U-B) \end{matrix} \right\} \quad \text{for} \quad \text{A1 Ib}\,.$$

Again, both methods (even considering an error in the UBV band fluxes of about 0.01 mag) deliver results that differ by a factor 2–3. This discrepancy in extinction implies that, obviously, the interstellar reddening is not the only extinction source acting on the observed UBV data. Instead, circumstellar material along the line of sight is causing an extinction of the stellar flux as well.

Possible circumstellar extinction sources might be, on the one hand, circumstellar dust with a wavelength dependent extinction behaviour different from the global interstellar one. On the other hand, since B[e] stars are known to have high mass loss rates, the circumstellar extinction might be caused by the high density wind that drops partly optically thick at optical and/or UV wavelengths.

To test which circumstellar extinction source might be acting on the UBV fluxes of S 23, we performed some simple test calculations for both scenarios. For the circumstellar dust scenario, we adopted a grain size distribution according to Mathis et al. (1977) for either silicates or amorphous carbon grains with SMC abundances of Si and C taken from Venn (1999). The optical depths of the circumstellar grains, resulting in a wavelength dependent dust extinction, are then calculated for the scenarios of an A0 Ib and an A1 Ib star. Interestingly, we found that neither the silicates nor the carbon grains (nor any combination of both) can account for the circumstellar extinction of S 23. We therefore conclude that circumstellar dust is most probably not the (major) source of the extra extinction. The location of the circumstellar dust around S 23, whose presence might be inferred from the IR photometry, should thus be out of the line of sight.

The situation is more complicated when the extinction is caused by the stellar wind. In this case, the wind not only absorbs and scatters the stellar light, instead it contributes with additional emission even at optical and UV wavelengths, as has recently been shown by Kraus et al. (2008b) for classical OB supergiants, and by Kraus et al. (2007) for the LMC B[e] supergiant R 126.

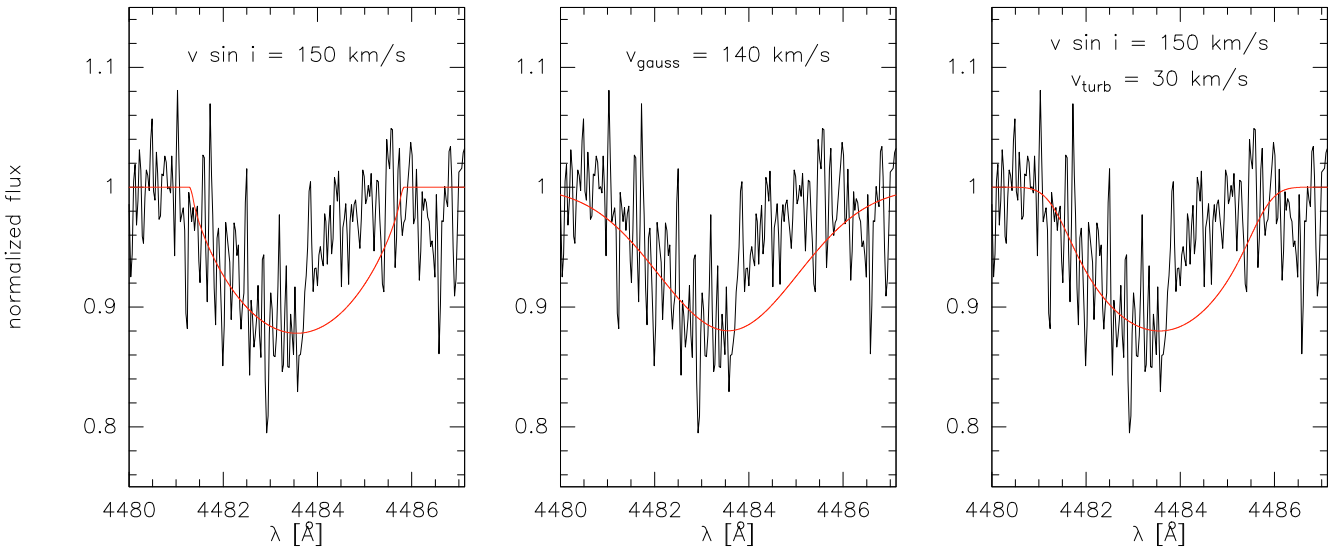

Fig. 4. Fitting process of the MgII λ4481 line with a pure rotation profile (*left panel*), a pure Gaussian profile (*mid panel*), and our best fit model (*right panel*) with a profile consisting mainly of stellar rotation plus some macro-turbulence.

We test the influence of the wind to the UBV band fluxes by assuming for simplicity (and since nothing is known about the real structure and geometry of the wind around S 23) a spherically symmetric isothermal wind, and calculate the wind contribution with the model of Kraus et al. (2008b). For the terminal wind velocity we use the escape velocity, which was found from observations of late B-type and early A-type supergiants by Lamers et al. (1995) to be a reasonable approximation. The only free parameter in the wind calculations is thus the mass loss rate, $\dot{M}$, which is varied over a certain range to calculate the wind extinction and emission in the UBV bands.

Interestingly, we could not constrain the circumstellar extinction for the scenario of an A0 Ib star, while the scenario of an A1 Ib star delivered reasonable values for both the mass loss rate, with $\dot{M} \simeq 3 \times 10^{-6}\ M_\odot\ \mathrm{yr}^{-1}$, and the interstellar extinction, with $E(B-V) \simeq 0.03$, constraining the classification of S 23 more towards an A1 star rather than an A0 star.

Compared to the value found from the observed $B-V$ color index, our value is slightly lower, indicating that the neglect of the wind influence to the emergent flux from the atmosphere leads to an overestimation of the real interstellar extinction. Such behaviour has also recently been found for classical B-type supergiants (Kraus et al. 2008a).

With the tentative classification of S 23 as A1 Ib star with an effective temperature of roughly 9000 K, and with the derived interstellar extinction of $A_V \simeq 0.10$, we find the following set of stellar parameters: $\log(L_*/L_\odot) \simeq 4.3$, $R_* \simeq 55$–$60\ R_\odot$, and, from the comparison with stellar evolutionary tracks calculated for SMC stars by Charbonnel et al. (1993), an initial mass of $M_{\rm ini} = 9.5 \ldots 11\ M_\odot$.

Finally, the small interstellar extinction value confirms the luminosity class adjustment of Ib, meaning that S 23 belongs to the group of low-luminosity B[e] supergiants, which has members in the LMC (Gummersbach et al. 1995) as well as in the Milky Way (Borges Fernandes et al. 2007), and which should probably be extended at least to early A-type stars.

5. Stellar rotation

With the classification of S 23 as an early A-type supergiant at the time of our observation, we next intend to determine its stellar rotation speed given by the parameter $v \sin i$. For late B-type and early A-type stars and supergiants, the most reliable photospheric line for the stellar rotation determination is the MgII λ4481 doublet (e.g., Royer 2005; Royer et al. 2002), which is also the only clearly detectable photospheric line in our spectra.

It has recently been shown that the Fourier analysis provides an excellent tool for the rotation velocity determination even for hot stars (see Royer 2005; Simón-Díaz & Herrero 2007). However, for the Fourier analysis to work properly, it is necessary to have data with extremely good S/N ratio because otherwise the noise level is too high to allow the zero points caused by the rotation profile to show up in the Fourier transform of the spectral data (Simón-Díaz & Herrero 2007). With the rather low S/N ratio of our FEROS data of the faint object S 23, the powerful Fourier analysis is thus not applicable. Instead, we have to rely on the less accurate full-width at half-maximum ($FWHM$) method to extract the possible stellar rotation of the star, i.e., we fit synthetic line profiles to the observed, normalised MgII line. The stellar rotation profile is described in the usual way (see, e.g., Gray 1976) with a limb-darkening coefficient of $\epsilon = 0.6$.

The line profile of the MgII λ4481 line appears to be asymmetric (see Fig. 4). However, this asymmetry is probably not real, but an artefact due to noise since only one of our spectra shows this asymmetry, while the other spectrum shows a symmetric line profile. For a proper $FWHM$ determination we therefore rely on the blue part of the line, only. Given the low S/N ratio, we derive a $FWHM$ of the observed MgII λ4481 line of 3.5 ± 0.1 Å. If we assume either a pure Gaussian profile or a pure rotation profile, we thus obtain maximum velocity values of $v_{\rm gauss} \simeq (140 \pm 5)\ \mathrm{km\,s^{-1}}$ and $v \sin i \simeq (150 \pm 5)\ \mathrm{km\,s^{-1}}$, respectively. However, both possibilities, i.e., either a pure Gaussian or a pure rotation profile, do not deliver satisfactory fits to the observed line profile (see left and middle panel of Fig. 4). While the edges are too sharp in the case of pure stellar rotation, the wings of the pure Gaussian are way too broad. Instead, a combination of both might be a good solution. But how can we estimate the individual amounts of the Gaussian and the rotational components?

It has been known for a long time that within the atmospheres of OBA supergiants some macroscopic line broadening occurs

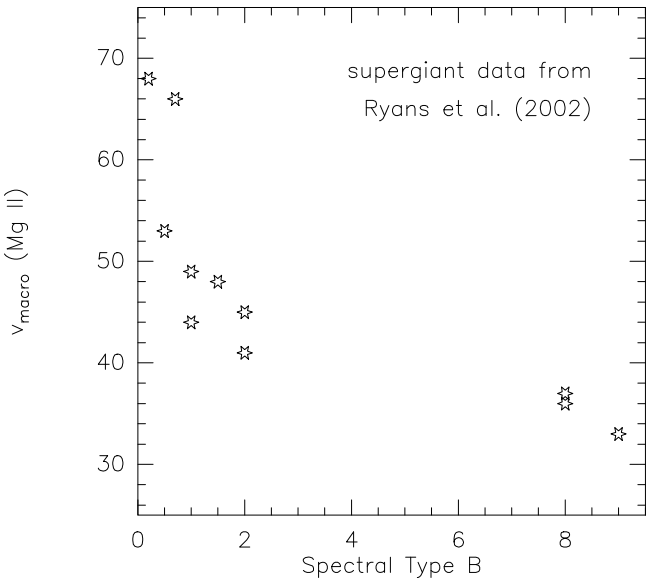

Fig. 5. Maximum velocity caused by macro-turbulence to the MgII λ4481 line for a sample of B-type supergiants. The data are taken from Ryans et al. (2002).

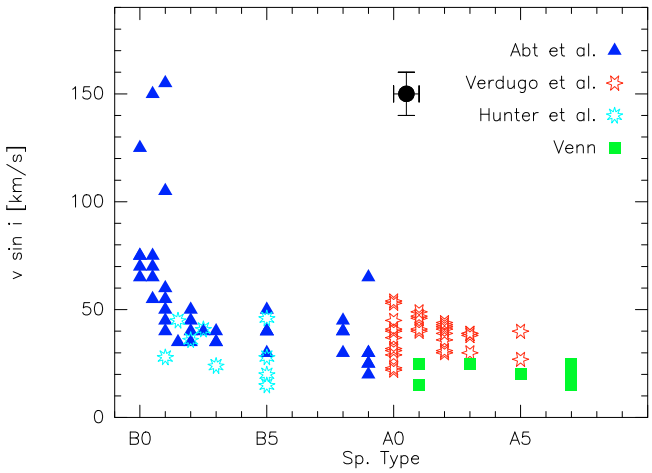

Fig. 6. Distribution of projected rotational velocities with spectral type of a sample of galactic (Abt et al. 2002; Verdugo et al. 1999) and SMC (Hunter et al. 2008; Venn 1999) supergiants. The big spot with errorbars is the value of S 23 derived from our analysis.

that is of no rotational origin. This broadening component can be described with a Gaussian profile and is usually referred to as (macro-)turbulence (see, e.g., Howarth 2004). This "extra" broadening of the photospheric lines is thereby not restricted to hydrogen and helium lines, but also appears in metal lines. The physical understanding and interpretation of this component is, however, still missing. In an attempt to determine the contribution of this macro-turbulence to line broadening, Ryans et al. (2002) investigated a sample of B-type supergiants trying to disentangle the contributions of rotation and macro-turbulence with high precision. One of the key lines in their investigation was the MgII λ4481 line. Inspection of their Table 3 reveals that there is an obvious trend between the maximum possible turbulent velocity and the effective temperature of the star. This is shown in Fig. 5, where we plotted the maximum turbulent velocity found for the sample supergiants of Ryans et al. (2002) versus spectral type of the stars. While for the early-type supergiants maximum macro-turbulence as high as 70 km s^{-1} might be present, it rapidly decreases towards the late type stars to about 30–35 km s^{-1} only. If this trend continues for the A-type supergiants, we might expect a maximum macro-turbulence of about 30 km s^{-1} acting on the photospheric lines of S 23.

We use this value of 30 km s^{-1} for the Gaussian profile and calculate the MgII λ4481 line profile by adjusting the rotational velocity such that the observed $FWHM$ is reproduced. Since the Gaussian velocity contribution is rather small, it does not significantly influence the total line width, which is still purely rotationally dominated with about the same value of $v \sin i \sim 150 \pm 5$ km s^{-1} as without macro-turbulence. The only influence of the Gaussian component concerns the line wings (see right panel of Fig. 4). Overall, this combination of rotation plus macro-turbulence gives a reasonably good fit to the observed line profile.

The value of $v \sin i$ found from our fitting is high when compared to the projected rotation velocities of normal galactic B and A-type supergiants, for which a tendency of decreasing rotation velocity with effective temperature is reported. This can be seen in Fig. 6, where we plot the results for four samples: (i) galactic B-type supergiants from Abt et al. (2002); (ii) galactic A-type supergiants from Verdugo et al. (1999); (iii) SMC B-type supergiants from Hunter et al. (2008); and (iv) SMC A-type supergiants from Venn (1999). The SMC stars turn out to have even smaller velocities than their galactic counterparts, but this effect might arise simply from small number statistics. Compared to the mean rotational velocity of the galactic and SMC late B-type and early A-type supergiants, the value derived for S 23 is clearly a factor of three higher.

However, as discussed already in the introduction, the B[e] phenomenon seems to be linked to rapid stellar rotation. For the class of the B[e] supergiants, only for three stars the value of $v \sin i$ could be derived so far. These are the LMC B[e] supergiants Hen S93 with $v \sin i \simeq 65$ km s^{-1} (Gummersbach et al. 1995) and R 66 with $v \sin i \simeq 50$ km s^{-1} (Zickgraf 2006), and the SMC B[e] supergiant R 50 with $v \sin i \simeq 150$ km s^{-1} (Zickgraf 2000). The latter one has a projected rotation speed on the same order as S 23, which is now the fourth B[e] supergiant with confirmed high projected rotational velocity. From our derived set of stellar parameters we can further estimate the critical velocity of the star, which turns out to be on the order of 200 km s^{-1}. This means, that S 23 is rotating with at least 75% of its critical velocity.

Interestingly, the optical spectrum of ZSW indicates that the MgII λ4481 line is less broad during the 1989 observations. A tentative derivation of its $FWHM$ delivers a value of (2.6 ± 0.2) Å. Neglecting any other broadening mechanism, this $FWHM$ value results in a maximum rotational velocity of $v \sin i \simeq 110 \pm 10$ km s^{-1}. This result is surprising, because it indicates that S 23 might not only have cooled, but at the same time also increased its projected rotational velocity by at least 35%.

6. Discussion

The investigation of our high-resolution optical spectra in combination with the photometric data of Massey (2002) resulted in the tentative classification of S 23 as a rapidly rotating A1 Ib star. On the other hand, our evaluation of the MgII/HeI line ratio derived (even though with large error bars) from the spectra of ZSW, delivered a spectral classification more consistent with a star of roughly spectral type B9 Ib. The most striking differences are thus an apparent temperature decrease by about 1500 K, based on the spectral type versus effective temperature

calibration of Evans & Howarth (2003), and shown in Fig. 3; and, even more curious, an increase in projected rotational velocity by about 35% (see previous section) within a time interval of only 11 years. In this section, we therefore investigate different scenarios that might explain this peculiar behaviour. For this, we first consider some natural possibilities like stellar evolution (Sect. 6.1) and mass ejection occulting the star in form of a shell phase as is often observed for the classical Be stars (Sect. 6.2). Since both attempts fail to explain the observed peculiar variations in S 23, we present and discuss in Sect. 6.3 further scenarios, which are more speculative. Of course, the amount and quality of our available data is definitely not sufficient for a proper analysis, which could lead to a discrimination between the different scenarios. Instead, we want to discuss qualitatively the expected observable effects for those scenarios that seem to be at least likely and worth further investigation.

6.1. Stellar evolution

The apparent cooling of the star in combination with a simultaneous speed-up of the rotation velocity is unexpected and surprising. The first scenario we might think of is stellar evolution. However, stellar evolution theories predict that when the star expands, i.e., cools, it can only *decrease* its rotation velocity. An *increase* in rotation speed during the post-main sequence evolution of a rapidly rotating star at SMC metallicity and with an initial mass of about 10 $M_\odot$ can only occur during the blue loop, i.e., while the star contracts and heats up again (Maeder & Meynet 2001). In addition, the timescales for such a star to cool from about 11 000 K to less than 9500 K is on the order of 5000 yr (Meynet, private communication). This is definitely longer than the one decade we found. The changes in the spectral appearance of S 23 can thus definitely not be explained by current theories of stellar evolution.

6.2. Comparison with shell formations of classical Be stars

A different interpretation of the apparent cooling might be given by the assumption of material ejection, e.g., in form of a ring or shell, leading to an (partly) occultation of the central star. Such phenomenon are known, e.g., from Be stars that can undergo a so-called shell phase (see, e.g., Hanuschik 1996; Porter & Rivinius 2003). The shell, ejected from the central star, thereby acts as an extinction source. Derivation of the stellar parameters from absorption lines created within such a shell can, therefore, result in much lower *apparent* effective temperature values than the real stellar one derived during a non-shell phase. Such a behaviour has been reported, e.g., for the Be shell star 4 Herculis, for which an apparent drop in effective temperature by 3000 K during the shell phase was found by Koubský et al. (1997). However, contrary to our target S 23, but in agreement with expected physical behaviour, the rotation velocity derived from the shell absorption line decreased as well. A shell phase of S 23, mimicking a temperature decrease, thus has severe problems in explaining our observations, even if the presence of some "shell-lines" (like the FeII and SiII lines) in our spectra hint towards the existence of a large amount of circumstellar material.

6.3. Possible (speculative) scenarios for S 23

Since neither stellar evolution, nor a high-density mass ejection in the form of a ring or shell can explain the peculiarities observed for S 23, we need to think of different mechanisms. In this section, we therefore present three alternative scenarios that might be worth further detailed investigation. These are (i) a high precession rate, (ii) an eclipsing binary, and (iii) surface He abundance and/or temperature inhomogeneities. All three are able to explain the peculiarities of S 23, and all three can be tested by future observations. But we want to stress again that these scenarios can only be considered as simplified models, given the quality of the available data.

6.3.1. Precession of the system

One possible explanation for the apparent cooling with increasing rotation velocity might be a precession of the star with respect to the line of sight. Since we know that S 23 is rapidly rotating, the classification of the star strongly depends on the inclination angle under which it is observed.

The effects of rapid stellar rotation are manifold. Rapid rotation leads to a deformation of the stellar surface in the form of flattening. Thus, the polar regions become much hotter than the equatorial region, which is usually referred to as gravity darkening. Depending on the fraction of the rotation velocity to the critical velocity, the difference between polar and equatorial effective temperature can exceed a factor of two. The same holds also for the other stellar parameters like the surface gravity, stellar flux, mass flux, and escape velocity.

From the differences in observed rotation velocity, $v \sin i$, we may conclude that the inclination of the system has increased between ZSW and our observations, which means, that the system was observed more edge-on in 2000 than in 1989. To quantify this, we take the values of $v \sin i = 110\ \mathrm{km\,s^{-1}}$ in 1989, and $v \sin i = 150\ \mathrm{km\,s^{-1}}$ in 2000. Then, the difference in inclination follows to

$$\sin i_{2000} = \frac{150}{110} \sin i_{1989} = 1.36 \sin i_{1989}, \quad (1)$$

which means that the inclination angle has increased by almost 40%. Assuming that the star was seen more or less edge-on (i.e., inclination angle of 90°) in 2000, it must thus have been seen under an inclination angle of about 47° in 1989. This conclusion is, however, only strictly valid, as long as the inclination did not cross the equatorial plane yet.

A lower limit to the inclination angle in 2000 is given by the critical rotation of the star, $v_{\mathrm{crit}} \simeq 200\ \mathrm{km\,s^{-1}}$. Assuming that the star is rotating at its critical speed, it delivers a minimum inclination angle of 48° in 2000, and of 35° in 1989.

To get a rough idea of the influence of the rapid rotation in combination with the postulated precession on the observable mean effective temperature, we consider the following scenario for S 23 (which need not be correct, but which is only meant to show the basic idea of this toy model).

Since rotation at the critical limit is not very realistic, we assume in the following that the star was seen more or less edge-on in 2000 so that S 23 rotates with 75% of its critical speed, i.e., $\omega = v_{\mathrm{eq}}/v_{\mathrm{crit}} = 0.75$. Such an edge-on scenario is not in contradiction with our results from Sect. 4, where we found that the dust is most probably not located along the line of sight. In fact, for rapidly rotating stars the mass loss happens much stronger via the poles than via the equatorial region, and to date models like, e.g., the wind-compressed disk (Bjorkman & Cassinelli 1993) failed in confining the material within the equatorial plane. In addition, spectropolarimetric observations of Bjorkman et al. (1998) for the galactic B[e] star HD 50138 have shown that the polarisation is mainly caused by scattering within an almost edge-on seen pure gaseous disk, while the huge amount of dust

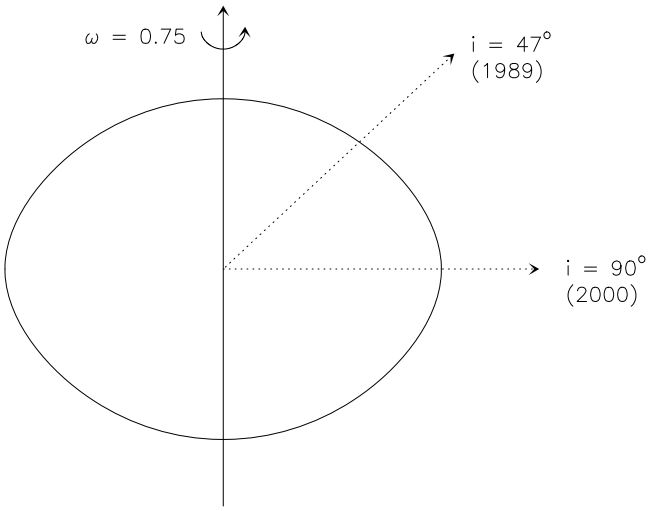

Fig. 7. Shape of S 23 rotating with 75% of its critical velocity. Also included are the assumed positions of the observers with respect to the rotation axis of the star in the two periods of optical observations.

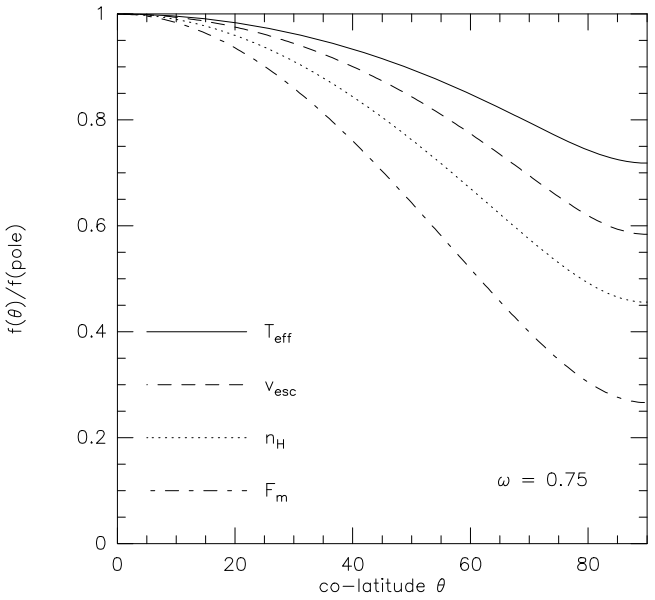

Fig. 8. Distribution of the surface parameters (effective temperature, escape velocity, hydrogen density, and mass flux) with co-latitude, θ, normalised to their polar values. All parameters are found to drop from pole to equator (for details on their calculation see Kraus 2006).

observed from this system seems not to be connected with the disk at all.

Following Kraus (2006), we compute the surface structure of the star rotating with $\omega = 0.75$ (shown in Fig. 7). For the adopted rotation speed, a deformation (i.e., flattening) of the stellar surface is obvious. Also included in this plot are the inclination angles under which the star might have been observed in 1989 and in 2000. While in 2000 most of the observed flux was emitted from the equatorial region with some minor contributions from higher altitudes, the flux observed in 1989 was emitted from an intermediate altitude, with contributions from both, the polar and the equatorial region.

To obtain an idea about the expected differences in the observed stellar spectra, we further calculate the surface distribution of the latitude dependent stellar parameters like effective temperature $T_{\rm eff}(\theta)$, escape velocity $v_{\rm esc}(\theta)$, mass flux $F_{\rm m}(\theta)$, and hydrogen desity $n_{\rm H}(\theta)$ for a star rotating with $\omega = 0.75$. These parameters are shown in Fig. 8 as a function of the co-latitude θ (i.e., $\theta = 0$ at the pole), normalised to their polar values. They are all found to decrease by non-negligible amounts from the pole to the equator.

In particular, we find from Fig. 8 the following behaviour of the effective temperature:

$$T_{\rm eff}(\theta = 47°) \simeq 0.91\, T_{\rm eff}(\theta = 0°), \quad (2)$$

$$T_{\rm eff}(\theta = 47°) \simeq 1.26\, T_{\rm eff}(\theta = 90°). \quad (3)$$

Since for an inclination of ~47° the stellar emission contains contributions from the hotter as well as from the cooler regions, we might assume that the effective temperature at $\theta = 47°$ is reflecting quite well the real observed spectrum. This means, that we can calculate the polar as well as the equatorial value of the effective temperature, resulting in $T_{\rm eff}(\theta = 0°) \simeq 12\,100$ K, and $T_{\rm eff}(\theta = 90°) \simeq 8700$ K. The equatorial value is somewhat lower than our effective temperature of 9 000 K derived from the FEROS spectrum. This is, however, no contradiction, because the real "observable" mean effective temperature under an edge-on inclination of the star will certainly be somewhat higher than the pure value at 90°, due to some contributions from higher altitudes. In addition, the temperature calibration of Evans & Howarth (2003) is certainly too coarse for a detailed temperature assignment.

In summary, the precession scenario might explain both, the apparent cooling with an increase in rotation velocity, just from an increase of the inclination axis of a rapidly rotating star from about 47° to about 90°. Whether such a strong precession will indeed occur, and what might be the reason for such rapid precession movement, is, however, not known.

To test the precession scenario, we would need to monitor the star over a period of several years to see whether the HeI lines re-appear (i.e., the star "heats up" again) with a simultaneous decrease of the projected rotation velocity measured from the MgII lines.

6.3.2. An eclipsing binary scenario

A second possible scenario to explain the strong variations observed in S 23 might be that of an eclipsing binary system, in which one component is perhaps a B9 Ib star and the other one perhaps a A1 Ib star. The disappearance of the HeI lines in our spectra might then be interpreted with the A1 Ib star occulting more or less the hotter B9 Ib component, while the spectra of ZSW, in which the HeI lines were present and strong, indicate that the hotter component was dominating the spectral appearance of the system.

To test the hypothesis of S 23 being an eclipsing binary, it is certainly useful to perform a high S/N monitoring of its few available photospheric lines, (i.e., the HeI lines and the MgII line). A further test for the eclipsing binary scenario would be the monitoring of its light curve. Since the hotter component is also expected to be the more luminous one, the system must appear fainter when the B9 star is eclipsed than when the A1 star is eclipsed.

6.3.3. A rapidly rotating star with surface inhomogeneities

A third quite interesting scenario is based on the assumption that S 23 might have a patchy surface abundance in He. The existence of such inhomogeneous or spotty surface patterns are known especially for some so-called chemically peculiar (CP)

stars (see, e.g., Smith 1996; Briquet et al. 2001, 2004; Lehmann et al. 2006; Krtička et al. 2007). These objects at or close to the main-sequence are supposed to be rigidly rotating, and the variations observed in their HeI line profiles are interpreted as abundance inhomogeneities in the form of large stellar spots that appear within and again disappear from the line of sight as the star revolves. In addition, these stars are found to possess longitudinal magnetic fields (e.g., Khokhlova et al. 2000; Briquet et al. 2007), and there seems to be evidence that variations in the magnetic field might be the cause for the abundance inhomogeneities.

Furthermore, the stellar surfaces of some of the CP stars seem to have temperature inhomogeneities (see, e.g., Böhm-Vitense & van Dyk 1987; Lehmann et al. 2006), and even the need of a co-existence of abundance and temperature inhomogeneities has recently been claimed by Lehmann et al. (2007), even though the physical processes resulting in such patchy surface structures are not understood at all.

S 23 is definitely not a main-sequence star, and to our knowledge, no such abundance or temperature inhomogeneities have been reported for a supergiant so far. In addition, nothing is known about a possible magnetic field on the surface of S 23. Nevertheless, such a surface inhomogeneity seems to be an interesting scenario, at least to explain the variations in the HeI lines. Whether this inhomogeneity can also explain the different observed values of $v \sin i$, needs to be investigated in more detail. At least the classical stellar rotation profile used in Sect. 5 to derive $v \sin i$ from the $FWHM$ will in such a scenario certainly not be valid anymore.

If S 23 possesses He spots, the variation of the HeI lines must be correlated to the rotation period of the star. Assuming that S 23 is seen edge-on, the derived value of $v \sin i = 150\,\mathrm{km\,s^{-1}}$ delivers the equatorial rotation velocity. With a radius of roughly 60 $R_\odot$, this results in a period of about 20 days. To prove or disprove the scenario of surface inhomogeneities in either He abundance, or temperature, or even both, one would need to monitor the HeI and MgII lines in the spectrum of S 23 over at least one rotational period.

7. Conclusions

We investigated the SMC star S 23, which was formerly classified by ZSW as a B8 Ib star, belonging to the class of B[e] supergiants. Our optical spectra show clear differences to the previously published one. These differences especially concern the absence of all photospheric HeI absorption lines. Our spectra are therefore consistent more with a spectral classification of S 23 as A1 Ib supergiant. This classification is further supported by our analysis of the photometric UBV data. During this analysis, we could derive self-consistently the contributions of the interstellar extinction, and of the circumstellar extinction caused by the stellar wind. A circumstellar extinction caused predominantly by dust could be excluded.

We further determined the projected rotation velocity of S 23 from an analysis of its photospheric MgII line. We found a value of $v \sin i \simeq 150\,\mathrm{km\,s^{-1}}$, which claims that S 23 is rotating with at least 75% of its critical velocity. Consequently, S 23 is the fourth member of the B[e] supergiant star group with confirmed high projected rotational velocity.

The most puzzling result is the fact that within a period of only 11 years, between the two sets of spectroscopic observations, the star seems to have cooled by more than 1500 K, and at the same time increased its rotation speed by about 35%. Such behaviour is definitely ruled out by any stellar evolution scenario. And also the scenario of a shell phase, as is often reported for classical Be stars, has severe difficulties in explaining all the observed peculiarities in S 23. Therefore, we presented and discussed several other alternatives: a rapidly rotating star undergoing a high precession, the scenario of an eclipsing binary, and the idea of He abundance and/or temperature inhomogeneities on the stellar surface, as they have been reported from CP stars. All these suggestions can explain most of the curiosities of S 23. However, the question, which of these scenarios is the correct one, or whether even all scenarios have to be discarded, could not be solved. Nevertheless, we suggested observational tests that can be performed to distinguish or discard the different scenarios. Definitely more observations with a much better time resolution are needed to disentangle the mystery of the peculiar variations in S 23.

Acknowledgements. We are greateful to Herman Hensberge and Georges Meynet for many fruitful discussions concerning the peculiarities of S 23, and to the anonymous referee for the helpful comments and suggestions. This research made use of the NASA Astrophysics Data System (ADS) and of the SIMBAD and 2MASS databases. M.K. acknowledges financial support from GA AV ČR number KJB300030701, and M.K. and J.K. from GA ČR number 205/08/0003. M.B.F. acknowledges financial support from the Belgian Federal Science Policy Office (Research Fellowship for non-EU Postdocs) and CNRS for the post-doctoral grant.

References

Abt, H. A., Levato, H., & Grosso, M. 2002, ApJ, 573, 359
Azzopardi, M. 1987, A&AS, 69, 421
Azzopardi, M., & Vigneau, J. 1982, A&AS, 50, 291
Bjorkman, J. E., & Cassinelli, J. P. 1993, ApJ, 409, 429
Bjorkman, K. S., Miroshnichenko, A. S., Bjorkman, J. E., et al. 1998, ApJ, 509, 904
Böhm-Vitense, E., & van Dyk, S. D. 1987, AJ, 93, 1527
Borges Fernandes, M., Kraus, M., Lorenz Martins, S., & de Araújo, F. X. 2007, MNRAS, 377, 1343
Bresolin, F., Pietrzyński, G., Urbaneja, M. A., et al. 2006, ApJ, 648, 1007
Bresolin, F., Urbaneja, M. A., Gieren, W., Pietrzyński, G., & Kudritzki, R.-P. 2007, ApJ, 671, 2028
Briquet, M., De Cat, P., Aerts, C., & Scuflaire, R. 2001, A&A, 380, 177
Briquet, M., Aerts, C., Lüftinger, T., et al. 2004, A&A, 413, 273
Briquet, M., Hubrig, S., Schöller, M., & De Cat, P. 2007, Astron. Nachr., 328, 41
Charbonnel, C., Meynet, G., Maeder, A., et al. 1993, A&AS, 101, 415
Curé, M. 2004, ApJ, 614, 929
Curé, M., Rial, D. F., & Cidale, L. 2005, A&A, 437, 929
Domiciano de Souza, A., Driebe, T., Chesneau, O., et al. 2007, A&A, 464, 81
Evans, C. J., & Howarth, I. D. 2003, MNRAS, 345, 1223
Evans, C. J., Howarth, I. D., Irwin, M. J., Burnley, A. W., & Harries, T. J. 2004, MNRAS, 353, 601
Gray, D. F. 1976, The observation and analysis of stellar photospheres (New York: Wiley)
Gummersbach, C. A., Zickgraf, F.-J., & Wolf, B. 1995, A&A, 302, 409
Hanuschik, R. W. 1996, A&A, 308, 170
Howarth, I. D. 2004, in Stellar Rotation, ed. A. Maeder, & P. Eenens (San Francisco: ASP), IAU Symp., 215, 33
Hubeny, I., & Lanz, T. 2000, SYNSPEC – A User's Guide
Hunter, I., Lennon, D. J., Dufton, P. L., et al. 2008, A&A, 479, 541
Johnson, H. L. 1966, ARA&A, 4, 193
Keller, S. C., & Wood, P. R. 2006, ApJ, 642, 834
Khokhlova, V. L., Vasilchenko, D. V., Stepanov, V. V., & Romanyuk, I. I. 2000, Astron. Lett., 26, 177
Koubský, P., Harmanec, P., Kubát, J., et al. 1997, A&A, 328, 551
Kraus, M. 2006, A&A, 456, 151
Kraus, M., & Miroshnichenko, A. S. 2006, Stars with the B[e] phenomenon, ASP Conf. Ser., 355 (San Francisco: ASP)
Kraus, M., Krügel, E., Thum, C., & Geballe, T. R. 2000, A&A, 362, 158
Kraus, M., Borges Fernandes, M., de Araújo, F. X., & Lamers, H. J. G. L. M. 2005, A&A, 441, 289
Kraus, M., Borges Fernandes, M., & de Araújo, F. X. 2007, A&A, 463, 627
Kraus, M., Borges Fernandes, M., & Kubát, J. 2008a, A&A, submitted
Kraus, M., Kubát, J., & Krtička, J. 2008b, A&A, 481, 499
Krtička, J., Mikulášek, Z., Zverko, J., & Žižňovský, J. 2007, A&A, 470, 1089
Kurucz, R. L. 1979, ApJS, 40, 1

Kurucz, R. L. 1993, Atomic Data for Opacity Calculations, Kurucz CD-ROM No. 1
Lamers, H. J. G. L. M., Snow, T. P., & Lindholm, D. M. 1995, ApJ, 455, 269
Lamers, H. J. G. L. M., Zickgraf, F.-J., de Winter, D., et al. 1998, A&A, 340, 117
Lehmann, H., Tsymbal, V., Mkrtichian, D. E., & Fraga, L. 2006, A&A, 457, 1033
Lehmann, H., Tkachenko, A., Fraga, L., Tsymbal, V., & Mkrtichian, D. E. 2006, A&A, 471, 941
Leitherer, C., & Wolf, B. 1984, A&A, 132, 151
Lennon, D. J. 1997, A&A, 317, 871
Lennon, D. J., Dufton, P. L., & Fitzsimmons, A. 1992, A&AS, 94, 569
Lennon, D. J., Dufton, P. L., & Fitzsimmons, A. 1993, A&AS, 97, 559
Maeder, A., & Meynet, G. 2001, A&A, 373, 555
Magalhães, A. M. 1992, ApJ, 398, 286
Magalhães, A. M., Melgarejo, R., Pereyra, A., & Carciofi, A. C. 2006, in Stars with the B[e] Phenomenon, ed. M. Kraus, & A. S. Miroshnichenko (San Francisco: ASP), ASP Conf. Ser., 355, 147
Massey, P. 2002, ApJS, 141, 81
Massey, P., Lang, C. C., DeGioia-Eastwood, K., & Garmany, C. D. 1995, ApJ, 438, 188
Mathis, J. S., Rumpl, W., & Nordsieck, K. H. 1977, ApJ, 217, 425
McGregor, P. J., Hillier, D. J., & Hyland, A. R. 1988a, ApJ, 334, 639
McGregor, P. J., Hyland, A. R., & Hillier, D. J. 1988b, ApJ, 324, 1071
McGregor, P. J., Hyland, A. R., & McGinn, M. T. 1989, A&A, 223, 237
Melgarejo, R., Magalhães, A. M., Carciofi, A. C., & Rodrigues, C. V. 2001, A&A, 377, 581
Morris, P. W., Eenens, P. R. J., Hanson, M. M., Conti, P. S., & Blum, R. D. 1996, ApJ, 470, 597
Porter, J. M., & Rivinius, Th. 2003, PASP, 115, 1153
Prévot, M. L., Lequeux, J., Maurice, E., et al. 1984, A&A, 132, 389
Royer, F. 2005, Mem. S. A. It. Suppl. 8, 124
Royer, F., Grenier, S., Baylac, M.-O., Gómez, A. E., & Zorec, J. 2002, A&A, 393, 897
Ryans, R. S. I., Dufton, P. L., Rolleston, W. R. J., et al. 2002, MNRAS, 336, 577
Sahai, R., Brillant, S., Livio, M., et al. 2002, ApJ, 573, L 123
Schmidt-Kaler, Th. 1982, in Landolt-Börnstein, New Series, Group IV, Vol. 2b, ed. K. Schaifers, & H. H. Voigt (Berlin: Springer, 1)
Simón-Díaz, S., & Herrero, A. 2007, A&A, 468, 1063
Skrutskie, M. F., Cutri, R. M., Stiening, R., et al. 2006, AJ, 131, 1163
Smith, K. C. 1996, Ap&SS, 237, 77
Venn, K. A. 1999, ApJ, 518, 405
Verdugo, E., Talavera, A., & Gómez de Castro, A. I. 1999, A&A, 346, 819
Verschueren, W. 1991, Ph.D. Thesis, Free University of Brussels, Belgium
Walborn, N. R. 1983, ApJ, 265, 716
Zickgraf, F.-J. 2000, in The Be Phenomenon in early-type stars, ed. M. A. Smith, H. F. Henrichs, & J. Fabregat (San Francisco: ASP), ASP Conf. Ser., 214, 26
Zickgraf, F.-J. 2006, in Stars with the B[e] Phenomenon, ed. M. Kraus, & A. S. Miroshnichenko (San Francisco: ASP), ASP Conf. Ser., 355, 135
Zickgraf, F.-J., Wolf, B., Stahl, O., Leitherer, C., & Klare, G. 1985, A&A, 143, 421
Zickgraf, F.-J., Wolf, B., Stahl, O., Leitherer, C., & Appenzeller, I. 1986, A&A, 163, 119
Zickgraf, F.-J., Wolf, B., Stahl, O., & Humphreys, R. M. 1989, A&A, 220, 206
Zickgraf, F.-J., Stahl, O., & Wolf, B. 1992, A&A, 260, 205 (ZSW)